Received: 18 January 2021 | Accepted: 5 May 2021

DOI: 10.1111/cpf.12708

REVIEW ARTICLE

Clinical Physiology and Functional Imaging

Cardiac perfusion by positron emission tomography

Wail Nammas[1] | Teemu Maaniitty[2] | Juhani Knuuti[2] | Antti Saraste[1,2]

[1]Heart Center, Turku University Hospital, Turku, Finland

[2]PET Centre, Turku University Hospital and University of Turku, Turku, Finland

Correspondence
Antti Saraste, Heart Center, Turku University Hospital, Turku, Finland.
Email: antti.saraste@utu.fi

Funding information
Turun Yliopistollinen Keskussairaala; Academy of Finland; Finnish Foundation for Cardiovascular Research; Hospital District of Southwest Finland

Abstract

Myocardial perfusion imaging (MPI) with positron emission tomography (PET) is an established tool for evaluation of obstructive coronary artery disease (CAD). The contemporary 3-dimensional scanner technology and the state-of-the-art MPI radionuclide tracers and pharmacological stress agents, as well as the cutting-edge image reconstruction techniques and data analysis software, have all enabled accurate, reliable and reproducible quantification of absolute myocardial blood flow (MBF), and henceforth calculation of myocardial flow reserve (MFR) in several clinical scenarios. In patients with suspected coronary artery disease, both absolute stress MBF and MFR can identify myocardial territories subtended by epicardial coronary arteries with haemodynamically significant stenosis, as defined by invasive coronary fractional flow reserve measurement. In particular, absolute stress MBF and MFR offered incremental prognostic information for predicting adverse cardiac outcome, and hence for better patient risk stratification, over those provided by traditional clinical risk predictors. This article reviews the available evidence to support the translation of the current techniques and technologies into a useful decision-making tool in real-world clinical practice.

KEYWORDS

chronic coronary syndromes, coronary artery disease, myocardial blood flow, positron emission tomography, myocardial perfusion imaging

1 | INTRODUCTION

Either non-invasive functional imaging of myocardial ischemia or coronary computed tomography angiography is recommended as an initial test in the diagnostic work-up of chronic coronary syndromes (CCS) in the current clinical practice guidelines of the European Society of Cardiology (class of recommendation I, level of evidence B) (Knuuti et al., 2020). Imaging of myocardial ischemia encompasses a wide array of modalities which evaluate myocardial perfusion and/or left ventricular regional wall motion, under rest and stress.

The conventional semi-quantitative assessment of relative regional myocardial perfusion is based on the assumption that the region of the myocardium with the highest tracer uptake has normal perfusion and therefore can be taken as a reference for the other regions. This methodology can miss global 'balanced' reduction of myocardial perfusion caused by obstructive 3-vessel epicardial coronary artery disease (CAD) or diffuse coronary microvascular dysfunction, and may underestimate the extent of myocardial ischemia in the presence of multi-vessel CAD (Berman et al., 2007; Knuuti & Saraste, 2012; Schindler et al., 2014). In contrast to the relative regional myocardial perfusion assessment

by conventional positron emission tomography (PET) or single photon emission computed tomography (SPECT), absolute quantification of the global and regional myocardial blood flow (MBF) by PET obviates the drawbacks of overlooking global reduction of myocardial perfusion or underestimating the true extent of myocardial ischemia in patients with multi-vessel or left-main CAD (Kajander et al., 2011; Ziadi et al., 2012) (Figure 1). Indeed, among the non-invasive functional imaging techniques, myocardial perfusion imaging (MPI) by PET stands out as a tool to rule-in or rule-out functionally significant CAD as demonstrated by invasive fractional flow reserve measurement among patients with a wide range of pre-test probabilities (Knuuti et al., 2018). Quantitative MPI by PET has recently been increasingly employed in clinical practice, being incorporated in diagnostic protocols of patients presenting with intermediate pre-test probability of obstructive CAD. Limiting factors for use of PET MPI include availability of scanners and tracers, and local personnel expertise. This review aims at providing an overview of MPI with PET focusing on advances in quantification of MBF by PET.

2 | MYOCARDIAL PERFUSION TRACERS

Characteristics of the commonly available myocardial perfusion tracers are summarized in Table 1 (Maddahi & Packard, 2014; Murthy et al., 2018). An ideal perfusion tracer should have a linear relationship of the tracer uptake (measured activity) as a function of MBF (Murthy et al., 2018). Unfortunately, the most widely available tracers have suboptimal first-pass extraction and/or retention at high flow rates, and consequently, non-linear MBF-uptake relationships, underestimating the true MBF at higher flow rates. Therefore, a flow-dependent correction factor is needed for mathematical modelling of high-flow-range MBF. Nonetheless, large correction factors would augment the noise of measurement, increasing the scatter of perfusion values at high-flow-range MBF.

2.1 | ^{82}Rubidium

^{82}Rubidium (^{82}Rb) is a potassium analogue that is actively taken up by the myocardium through the membrane Na-K-adenosine triphosphatase (Maddahi & Packard, 2014). The physical half-life of ^{82}Rb is short, and it can be produced from local ^{82}Sr/^{82}Rb generators lasting 4–8 weeks (Yu et al., 2007). Since it does not need onsite cyclotron, it is the most widely used tracer for PET MPI, but requires high patient throughput for cost-effectiveness. For logistic reasons, only pharmacological stress can be used with a protocol employing ^{82}Rb PET MPI. On the other hand, the short half-life of ^{82}Rb enables fast rest–stress imaging protocols. Although the long positron range of ^{82}Rb would hamper image spatial resolution, the latter is enhanced by image reconstruction post-filtering and cardiorespiratory motion detection techniques.

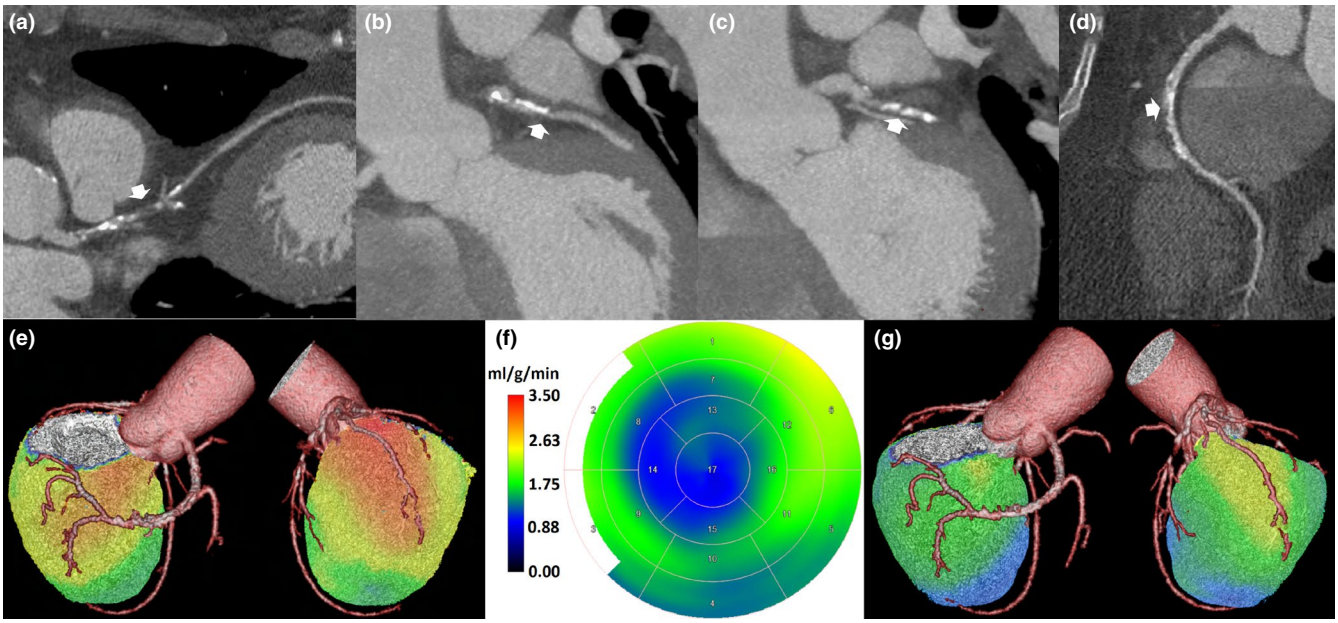

FIGURE 1 Quantitative myocardial blood flow in multi-vessel coronary artery disease: a middle-aged man with hypertension, dyslipidaemia, and family history of coronary artery disease complained of exertional angina, and exercise ECG showed 2-mm ST segment depression. Coronary computed tomography angiography showed total occlusion of the left anterior descending coronary artery (a), and calcification with suspected stenosis of the intermediate (b), left obtuse marginal (c), and right coronary artery (d) (arrows). Quantitative ^{15}O-water positron emission tomography revealed reduced stress myocardial blood flow in all coronary artery territories (f, polar map; g, 3D reconstruction), suggesting 3-vessel coronary artery disease. For comparison, the same perfusion image is presented on a relative scale, revealing only the most severely reduced perfusion in the territory of the distal left anterior descending coronary artery (e, 3D reconstruction). Subsequent invasive coronary angiography confirmed significant 3-vessel coronary artery disease, and the patient underwent revascularization

TABLE 1 Commonly used radionuclide tracers for myocardial perfusion imaging with positron emission tomography (Maddahi & Packard, 2014; Murthy et al., 2018)

Property	^{82}Rubidium	^{13}N-ammonia	^{15}O-water	^{18}F-flurpiridaz
Physical half-life	76 s	9.96 min	2.06 min	109 min
Positron range (millimeter)	8.6	2.53	4.14	1.03
Production equipment	Generator	Onsite or nearby cyclotron	Onsite cyclotron	Regional cyclotron
Extraction fraction at rest flow (0.75–1 ml/g/min)	70%	100%	100%	100%
Retention at rest flow (0.75–1 ml/g/min)	70%	90%	0%	90%
Extraction fraction at stress flow (3–4 ml/g/min)	35%	95%	100%	95%
Retention at stress flow (3–4 ml/g/min)	25%	50%	0%	55%
Rest/Stress dose for 2-dimensional PET (MBq)	1665	555	1110	111/259
Rest/Stress dose for 3-dimensional PET (MBq)	1110	370	740	74/222
Effective radiation dose (mSv)	1–4	1–2	1–2[a]	6
Image resolution	Lowest	Intermediate-high	Intermediate	Highest
Spillover from adjacent organs	Stomach wall	Liver and lungs	Liver	Liver
Treadmill exercise imaging protocol	Not feasible	Feasible/not practical	Not feasible	Feasible
Approval state	FDA-approved	FDA-approved	Not FDA-approved[b]	Phase III trials

Abbreviation: FDA, Food and Drug Administration.

[a]<0.5 mSv with new scanners and injected activity about 500 MBq.

[b]Clinically used in some European centers.

The effective radiation dose is low due to the short half-life of ^{82}Rb. Theoretically, the suboptimal and non-linear extraction fraction of ^{82}Rb makes it far from ideal tracer for MBF quantification; however, evidence supports the feasibility, accuracy and reproducibility of quantitative MPI with ^{82}Rb PET using the single-tissue compartment model, being validated against microspheres in a canine model of CAD (Anagnostopoulos et al., 2008; El Fakhri et al., 2009; Lautamäki et al., 2009; Lortie et al., 2007).

2.2 | ^{13}N-Ammonia

^{13}N-ammonia enters the myocardium by passive free diffusion across the sarcolemma, where it equilibrates with cytoplasmic ammonium, and gets trapped in the cytoplasm through conversion to ^{13}N-glutamine by glutamine synthase (Krivokapich et al., 1982). The half-life of ^{13}N-ammonia (almost 10 min) allows for its production in a nearby cyclotron (Maddahi & Packard, 2014). Although physical exercise test was described with ^{13}N-ammonia PET MPI, this approach is less practical for routine clinical practice. The relatively short positron range of ^{13}N-ammonia implies good spatial resolution. The extraction fraction of ^{13}N-ammonia is high, but flow-dependent correction is used with the high-flow-range MBF. Both the single- and two-tissue compartment models have been validated for quantification of MBF with ^{13}N-ammonia PET MPI, and the two-tissue compartment model takes into account the myocardial metabolic trapping (De Grado et al., 1996; Hutchins et al., 1990; Muzik et al., 1993). On the other hand, the high retention of ^{13}N-ammonia in the myocardium also allows for good quality of myocardial perfusion images (Saraste et al., 2012).

2.3 | ^{15}O-Water

Being metabolically inert and freely diffusible, ^{15}O-water enters the myocardium by passive diffusion; and since it does not accumulate in the myocardium, both wash-in and wash-out are applied for absolute MBF quantification, and parametric images are used for interpretation (Harms et al., 2011). Due to its short half-life, it needs onsite cyclotron for its production, and only pharmacological stress is feasible; however, it enables fast rest–stress imaging protocols. Yet, stress-only imaging could be sufficient for most patients with suspected obstructive CAD (Joutsiniemi et al., 2014). ^{15}O-water has an excellent first-pass extraction fraction that is independent on flow rate, and correction is not required; therefore, its kinetics are best described with single-tissue compartment models (Iida et al., 1988). Regional tracer uptake is directly proportional to segmental MBF, and this makes adequate contrast between segments supplied by normal and those supplied by stenosed coronary arteries (Danad et al., 2014). Indeed, ^{15}O-water PET is nowadays considered the gold standard of non-invasive MBF quantification. With the recent scanner technology, an injected activity near 500 MBq can be

adequate for ^{15}O-water MPI, with a consequent effective radiation dose below 0.5 mSv (Danad et al., 2014).

2.4 | ^{18}F-Flurpiridaz

A novel ^{18}F-labelled tracer ^{18}F-flurpiridaz binds to and competitively inhibits NADH:ubiquinone oxidoreductase (mitochondrial complex 1) in the mitochondria, without compromising cardiomyocyte viability (Yalamanchili et al., 2007). Kinetics can be expressed with a two-tissue compartment model (Saraste et al., 2012). Its long half-life allows for unit dose delivery from a regional cyclotron, obviating the need for an onsite cyclotron or a costly generator. The short positron range contributes to its excellent spatial resolution.

Preclinical studies demonstrated high flow-independent first-pass extraction fraction, which holds promise of a linear correlation between MBF and tracer uptake (Huisman et al., 2008). In an in vivo rat model, *^{18}F-Flurpiridaz* adequately delineated perfusion defects after permanent coronary occlusion (Higuchi et al., 2008; Sherif et al., 2009). In a pig model, ^{18}F-Flurpiridaz uptake and modelled MBF correlated with radioactive microsphere-derived MBF over a wide range of MBF under rest and pharmacological stress (Nekolla et al., 2009; Sherif et al., 2011). Despite the nearly 2-h half-life, Guehl et al. demonstrated the feasibility of a single-day rest–stress imaging protocol that can be achieved in <15 min, in a porcine model (Guehl et al., 2017). In a phase I clinical trial involving a rest-only protocol, *^{18}F-Flurpiridaz* showed adequate delineation of the myocardium up to 5 h post-injection, and the tracer was well tolerated by all subjects (Maddahi et al., 2011). In another phase I trial, excellent image quality was obtained with a high target-to-background ratio, after *^{18}F-Flurpiridaz* injection at rest, at peak adenosine stress, as well as at peak treadmill exercise, in a 2-day rest–stress protocol (Maddahi et al., 2009). The relatively long half-life of *^{18}F-Flurpiridaz* allowed for performance of a treadmill exercise imaging protocol (Maddahi et al., 2019; Maddahi et al., 2009). It was determined based on the relationship between rest–stress contamination and dosing that for a single-day rest–stress protocol, a minimum dose ratio of 3 was needed, with a 60-min waiting time between the two injections (for rest-adenosine stress protocol, 30-min waiting time); these protocols were implemented in phase II and III trials (Maddahi & Packard, 2014). Dosimetry suggested that injection of up to 518 MBq of *^{18}F-Flurpiridaz* during a rest–stress protocol would provide an acceptable effective radiation dose of 6.4 mSv (Maddahi et al., 2009). The heart received the largest mean absorbed dose with both exercise and adenosine stress, and the tracer was well tolerated by all subjects (Maddahi et al., 2019).

First-in-human quantification of MBF by *^{18}F-Flurpiridaz* during rest-adenosine stress protocol was feasible and revealed significant difference of MBF and myocardial flow reserve (MFR) between myocardial segments subtended by normal/mildly diseased arteries and those subtended by diseased (≥50% stenosis) arteries (Packard et al., 2014). In a phase II trial comparing visual analysis of ^{18}F-*Flurpiridaz* PET vs. *^{99m}Tc-Sestamibi* SPECT during a rest–stress protocol, the certainty of interpretation was considerably higher for ^{18}F-*Flurpiridaz* PET; PET had a higher sensitivity for detection of significant coronary lesions (by invasive coronary angiography (ICA)) than SPECT; the specificity was similar (Berman et al., 2013). A completed phase III multicentre trial ($n = 276$) established the diagnostic performance of ^{18}F-Flurpiridaz PET MPI in a single-day rest–pharmacological stress imaging protocol, taking quantitative coronary angiography (QCA) as the reference standard (Maddahi et al., 2020). In a recently published post-hoc analysis of that trial, both (per-vessel) stress MBF and MFR adequately identified obstructive CAD and were inversely related to the coronary stenosis severity. Both stress MBF and MFR obtained by ^{18}F-flurpiridaz PET agreed with the literature-reported typical values for the other tracers, and added incremental diagnostic value beyond clinical characteristics and relative MPI analysis (Moody et al., 2020). Another phase III trial is currently underway, which investigates the diagnostic efficacy of ^{18}F-Flurpiridaz PET MPI in a rest–pharmacological stress imaging protocol, compared with *^{99m}Tc-Sestamibi* SPECT, taking QCA as the reference standard, in patients with suspected CAD (NLM identifier: NCT03354273).

3 | MYOCARDIAL PET PERFUSION SCANNERS

Current PET MPI scanners employ 3-dimensional image acquisition mode, and require lower injected tracer activity; and therefore, lower effective radiation dose for the patient (Murthy et al., 2018). The injected dose needs to be carefully optimized: it should not be too high to avoid detector saturation during the first-pass extraction phase; and in the meantime, it should not be too low to preserve adequate tracer activity in the retention phase so as to maintain image quality. Weight-based tracer activity calculation could result in accurate MBF quantification with consistent image quality (Renaud et al., 2017).

4 | IMAGING PROTOCOLS

Traditionally, rest image acquisition is followed by stress image acquisition in the same day (rest–stress protocol), or occasionally next day for tracers with a long half-life. The time interval between the two scans depends on the tracer half-life. For tracers with a short half-life, such as ^{82}Rb and ^{15}O-water, the second (stress) image sequence can be started immediately after completion of the first (rest). Such time interval is 30 min in case of ^{13}N-ammonia MPI, to allow for tracer decay. The total scan time is in the order of 30 min for ^{82}Rb and ^{15}O-water, and 80 min for ^{13}N-ammonia. Stress-rest imaging protocol is also feasible, although it is unclear whether post-ischemic stunning from the stress imaging session can affect rest MBF with such protocol.

Evidence suggests that a protocol of stress-only MBF could be accurate and sufficient for detection of CAD (Danad et al., 2014; Hajjiri et al., 2009; Joutsiniemi et al., 2014; Kajander et al., 2011).

Such a protocol offers a simple approach with a shorter duration, and a lower effective radiation dose. Additionally, it is appropriate for patients with high resting MBF (women, heart transplant recipients) in whom MFR is reduced despite normal hyperaemic MBF, and it is not affected by the variability of resting MBF due to hemodynamic factors (McGinn et al., 1990). On the other hand, rest MBF is needed in patients with prior myocardial infarction to discriminate reversible myocardial ischemia from a permanent perfusion defect due to prior infarction. In a system that supports list-mode acquisition, PET data collected in the ECG-gated mode can offer simultaneous evaluation of the regional and global left ventricular systolic function from the same perfusion data set, especially when ^{15}O-water is not used as a tracer.

5 | IMAGE ACQUISITION AND ANALYSIS

A low-dose computed tomography (CT) scan for attenuation correction is obtained before dynamic or list-mode PET acquisition scan (emission scan) is acquired. This quality control step is critical to ensure optimal alignment between the attenuation correction and emission scan data sets, and misalignment, if any, should be corrected (Gould et al., 2007; Rajaram et al., 2013). Practically, all clinical PET MPI studies are acquired using dynamic or list-mode data collection which enables modelling of absolute MBF. The quantification of MBF requires measurement of arterial blood tracer activity over time for construction of time–activity curves from regions-of-interest (ROIs) located in the arterial blood pool. As only the portion of tracer that is free in plasma is available for myocardial tissue exchange, corrections may be used to account for red cell uptake, haematocrit, plasma protein binding, and tracer-labelled metabolites released in blood depending on tracer (Keiding et al., 2010). Dynamic frame rates are acquired over a range of 5–10 s for the first-pass phase, and 1–5 min for the retention phase. List-mode acquisition is generally recommended, as it allows flexibility in the timing and reconstruction of static, dynamic, ECG- and respiratory-gated images. Time–activity curves are then fit to a tracer-specific mathematical model that best describes the tracer kinetics. The most commonly used models are the single-tissue compartment model and the simplified retention model (Iida et al., 1988; Yoshida et al., 1996). Both models retain the property of normalizing the retention phase myocardial activity to account for the total activity delivered by the arterial blood, such that the zones of highest activity in the retention phase are scaled to 100%. The models typically include correction for the tracer-specific extraction fraction (which is in turn dependent on MBF and permeability-surface area product), regional correction for the total blood volume, and partial volume underestimation of myocardial tracer activity (Murthy et al., 2018). For ^{18}F-*Flurpiridaz*, a simplified approach was proposed based on measurement of the tracer retention (tracer activity divided by the integral of the arterial input function curve) and the standardized uptake value (SUV) during the retention phase showing adequate correlation with MBF measured with three-compartment model, and with microsphere-derived MBF in a porcine model (Sherif et al., 2011). This method would simplify the rest–stress protocols by obviating the need for tracer kinetic model analysis and first-pass transit imaging, but further validation is needed for this approach.

6 | PITFALLS IN IMAGE ACQUISITION, RECONSTRUCTION AND ANALYSIS

For accurate quantification of MBF, verification of correct acquisition and analysis of dynamic image series is of paramount importance. It is crucial to keep the position of the patient between the attenuation correction and PET emission scans. Any patient motion between the first-pass transit phase and the late retention phase must be detected and corrected; otherwise, estimated MBF measurements could be biased (Hunter et al., 2016). Dynamic time–activity curves must include a baseline zero frame to ensure adequate sampling of the arterial blood input function. The presence of multiple or broad peaks in the arterial blood pool time–activity curves may result from poor-quality injection, due to bad-fitting cannulas, arm position, etc. Additionally, the peak heights of the time–activity curves of the arterial blood pool during rest and stress should be comparable, provided that similar tracer activities were injected. Significant differences of peak activity between rest and stress time–activity curves might suggest tracer extravasation or incomplete delivery, and can lead to erroneous estimation of MBF values (Murthy et al., 2018). Since the resting MBF linearly correlates with the heart rate-pressure product, variability of the resting MBF should be accounted for during interpretation of MFR values (Saraste et al., 2012). Stress MBF values should always be considered to mitigate the confounding effect of resting MBF variability on the calculated MFR (Johnson & Gould, 2011). Variations in the tracer injection profile might compromise the reproducibility of MBF quantification, especially when a simplified retention model is employed for tracer fitting (Klein et al., 2018). Yet, although standardized software analysis methodology was described for both ^{13}N-ammonia and ^{82}Rb, considerable variation among commercially available software products still exists (Dekemp et al., 2013; Nesterov et al., 2014; Slomka et al., 2012; Tahari et al., 2014). For dynamic data set acquisition, iterative reconstruction is preferred as recommended by the manufacturer, and minimal smoothing is preferred for MBF quantification.

7 | STRESS TEST

Although exercise stress provides information on functional capacity and exercise-induced ST-segment changes, it is largely impractical with most of the currently used PET tracers for logistic reasons. Dynamic first-pass images must be acquired with the patient already in the scanner gantry at the time of tracer injection. Moreover, pharmacological stress achieved greater stress MBF rates than those obtained with isometric handgrip exercise (Brown et al., 1981). Two prior studies described the use of supine bicycle exercise

with ^{13}N-ammonia PET (Krivokapich et al., 1989; Tamaki et al., 1985). However, patient motion artefacts are potential source of error, and this protocol is hard to achieve with the long gantries of the current PET/CT scanners. A previous study reported larger perfusion defects with treadmill exercise than with dipyridamole stress with ^{13}N-ammonia PET; however, such protocol does not permit dynamic image acquisition for MBF quantification (Chow et al., 2006).

The standard preparation for pharmacological stress includes 4-h fast and abstinence from smoking, and at least 12-h abstinence from caffeine ingestion (24-h abstinence may be preferred) before vasodilator stress (Lapeyre et al., 2004; Murthy et al., 2018). Conventional vasodilators (dipyridamole, adenosine) have long been successfully employed with the currently used PET MPI tracers (Al-Mallah et al., 2010; Kajander et al., 2010). The more recent vasodilator regadenoson (a selective adenosine A2A receptor agonist approved by the US Food and Drug Administration in 2008) demonstrated high efficacy for detection of CAD with ^{82}Rb PET (Hsiao et al., 2013), although it achieved only 80% of the dipyridamole-induced hyperaemic MBF that was further increased to 90% by delaying ^{82}Rb injection (Johnson & Gould, 2015). Currently, the impact of regadenoson on absolute MBF is not well known. Nevertheless, both the overall and high-grade atrioventricular block were remarkably less frequent with regadenoson, compared with adenosine in a recent meta-analysis of SPECT studies (Andrikopoulou et al., 2019). When there is contraindication for vasodilator stress, dobutamine infusion (± atropine to augment heart rate response) according to the standard protocol can achieve hyperaemic MBF comparable to that induced by intracoronary adenosine in vessels with epicardial coronary stenosis, and to that of dipyridamole in healthy volunteers (Bartunek et al., 1999; Tadamura et al., 2001). Hyperaemic MBF induced by standard-dose dipyridamole infusion was not enhanced with high-dose dipyridamole, and was lessened with the addition of isometric handgrip (Czernin et al., 1995). Reversal of hyperaemia induced by pharmacological stress can be allowed 3–4 min after imaging was commenced without compromising image quality or the accuracy of MBF quantification.

8 | DIAGNOSTIC VALUE OF PET MPI

The diagnostic performance of conventional semi-quantitative PET MPI was previously demonstrated in comparison with SPECT MPI and cardiac magnetic resonance (Jaarsma et al., 2012; Mc Ardle et al., 2012). In one meta-analysis (15 studies, 1319 patients), conventional PET had a significantly higher diagnostic accuracy, compared with SPECT, both in per-patient and per-vessel analyses; the superior diagnostic accuracy of PET remained in most subgroups (Jaarsma et al., 2012). Moreover, the diagnostic performance of PET was similar to that of cardiac magnetic resonance (Jaarsma et al., 2012). In another meta-analysis (15 studies, 1344 patients) which included more recent literature, conventional ^{82}Rb PET had a superior diagnostic accuracy in comparison with ^{99m}*Tc-Sestamibi* SPECT, with both ECG-gating and attenuation correction, although the included studies did not directly compare the two diagnostic modalities (Mc Ardle et al., 2012).

Evidence supporting the diagnostic value of quantitative PET MPI parameters is summarized in Tables 2 and 3. The most thoroughly investigated quantitative parameters are hyperaemic MBF and MFR, over a range of cut-off values tested against various reference standards derived from ICA, with FFR ≤0.80 included in most of the studies. Overall, the per-patient sensitivity and specificity for detection of haemodynamically significant CAD ranged from 76 to 95% and from 83 to 91%, respectively, for hyperaemic MBF, and from 76 to 96% and from 36 to 88% respectively, for MFR. On the other hand, the corresponding per-vessel values ranged from 71 to 95% and from 70 to 92%, respectively, for hyperaemic MBF, and from 62 to 91% and from 66 to 87%, respectively, for MFR (Tables 2 and 3).

In the studies which compared head-to-head the diagnostic accuracy of hyperaemic MBF and MFR, both the per-patient and per-vessel sensitivity and specificity were overall better for hyperaemic MBF vs. MFR (FFR was included in the reference standard in 4 out of 5 studies) (Danad et al., 2013; Danad et al., 2014; Hajjiri et al., 2009; Joutsiniemi et al., 2014; Lee et al., 2016). Thus, the weight of evidence suggests a better diagnostic performance for standalone hyperaemic MBF than MFR. Notably, MFR is dependent on resting MBF, which in turn correlates linearly with the heart rate-pressure product (Gould et al., 1990; McGinn et al., 1990). Hemodynamic variables have much more impact on resting rather than hyperaemic MBF, and therefore cause greater variability of resting MBF, and consequently, MFR (Gewirtz, 2019; McGinn et al., 1990).

A meta-analysis exploring the diagnostic accuracy of MPI by different modalities (including hyperaemic MBF by PET) for detection of FFR-determined obstructive CAD reported a patient-level pooled sensitivity and specificity of 84% (95% CI 75–91%) and 87% (95% CI 80–92%), respectively; the corresponding vessel-level values were 83% (95% CI 77–88%) and 89% (95% CI 86–91%), respectively (Takx et al., 2015). Notably, this meta-analysis included 3 PET studies (290 patients, 870 vessel), of which per-patient values were reported for two studies only, and reported the diagnostic accuracy for different regional hyperaemic MBF cut-off values (range 1.86–2.5 ml/g/min) (Danad et al., 2013; Kajander et al., 2011; Lee et al., 2016). More recently, another meta-analysis evaluated different non-invasive testing modalities for detecting anatomically and functionally significant CAD, reporting patient-level pooled sensitivity of 89% (95%CI 82–93%) and specificity of 85% (95%CI 81–88%) for PET MPI in detection of FFR-determined functionally significant CAD (Knuuti et al., 2018).

There is no widely acknowledged optimal cut-off value of hyperaemic MBF or MFR for identifying obstructive CAD that fits all PET MBF tracers. Published data included heterogeneous cohorts with different prevalence of CAD, different reference standards for defining haemodynamically significant lesions (QCA, FFR), different tracers analysed with different software, and ultimately an array of cut-off values (mostly representing vascular territory values) for both hyperaemic MBF (range 1.85–2.5 ml/g/min) and MFR (range

TABLE 2 Characteristics of studies which employed hyperemic MBF in the diagnosis of angiographically and/or functionally significant CAD

Study	Year	Cohort size	Age (years)	Men (%)	Selection criterion	CAD (%)	Tracer	Stressor	Hyperemic MBF cutoff	Reference standard	Per-patient sensitivity (%)	Per-patient specificity (%)	Per-vessel sensitivity (%)	Per- vessel specificity (%)
Hajjiri et al.	2009	27	58	74.1	Known or Suspected CAD	70.4	^{13}N-ammonia	Adenosine	<1.85 in a vascular territory	ICA 70% lesion	NA	NA	81	85
Kajander et al.	2011	104	63.6	59.8	Suspected CAD	36.5	^{15}O-water	Adenosine	<2.5 in a vascular territory	FFR ≤ 0.8 or QCA 50% lesion	95	91	95	92
Danad et al.	2013	120	61	64.2	Suspected CAD	40.8	^{15}O-water	Adenosine	≤1.86 in ≥2 adjacent segments	ICA 50% lesion or FFR ≤ 0.8	76	83	71	89
Joutsiniemi et al.	2014	104	64	61.5	Suspected CAD	33.7	^{15}O-water	Adenosine	<2.4 in a vascular territory	QCA 50% lesion or FFR < 0.8	95	89	89	90
Danad et al.	2014	281	61	58.2	Suspected CAD	41	^{15}O-water	Adenosine	<2.3 in ≥2 adjacent segments	FFR ≤ 0.8/ICA 90% lesion	89	84	87	85
Lee et al.	2016	130	64.2	89.2	Known or Suspected CAD	30.6	^{13}N-ammonia	Adenosine	<1.99 in a vascular territory	FFR ≤ 0.8	NA	NA	78	73
Danad et al.	2017	204	58	63.5	Suspected CAD	44.2	^{15}O-water	Adenosine	<2.3 in ≥2 adjacent segments	FFR ≤ 0.8/ICA 90% lesion	87	84	81	75

Abbreviations: CAD, coronary artery disease; FFR, fractional flow reserve; ICA, invasive coronary angiography; MBF, myocardial blood flow; NA, not available; QCA, quantitative coronary angiography.

TABLE 3 Characteristics of studies which employed MFR in the diagnosis of angiographically and/or functionally significant CAD

Study	Year	Cohort size	Age (years)	Men (%)	Selection criterion	CAD (%)	Tracer	Stressor	MFR cutoff	Reference standard	Per-patient sensitivity (%)	Per-patient specificity (%)	Per-vessel sensitivity (%)	Per-vessel specificity (%)
Hajjiri et al.	2009	27	58	74.1	Known or Suspected CAD	70.4	^{13}N-ammonia	Adenosine	<2 in a vascular territory	ICA 70% lesion	NA	NA	62	85
Fiechter et al.	2012	73	61	73	Known or Suspected CAD	72.6	^{13}N-ammonia	Adenosine	<2 global/ vascular territory	ICA 50% lesion	96[a]	80[a]	91[a]	71[a]
Ziadi et al.	2012	120	63	73.3	Known or Suspected CAD	21[b]	^{82}Rb	Dipyridamole	<2 global MFR	ICA[b]	88[b]	51[b]	NA	NA
Morton et al.	2012	38	63	78	Known or Suspected CAD	84.2	^{13}N-ammonia	Adenosine	Regional MFR[c] <1.44	ICA 70% lesion	NA	NA	82	87
Danad et al.	2013	120	61	64.2	Suspected CAD	40.8	^{15}O-water	Adenosine	≤2.3 in ≥2 adjacent segments	ICA 50% lesion or FFR ≤ 0.8	76	63	73	75
Joutsiniemi et al.	2014	104	64	61.5	Suspected CAD	33.7	^{15}O-water	Adenosine	<2.5 in a vascular territory	QCA 50% lesion or FFR < 0.8	87	88	80	87
Danad et al.	2014	281	61	58.2	Suspected CAD	41	^{15}O-water	Adenosine	<2.5 in ≥2 adjacent segments	FFR ≤ 0.8/ICA 90% lesion	86	72	80	82
Naya et al.	2014	290	65	53.4	Suspected CAD	18.9[d]	^{82}Rb	Adenosine/ dipyridamol/ regadenoson	<1.93 global MFR	ICA[d]	89[d]	36[d]	NA	NA
Lee et al.	2016	130	64	89.2	Known or Suspected CAD	30.6	^{13}N-ammonia	Adenosine	<2.12 in a vascular territory	FFR ≤ 0.8	NA	NA	70	66

Abbreviations: CAD, coronary artery disease; FFR, fractional flow reserve; ICA, invasive coronary angiography; MFR, myocardial flow reserve; NA, not available; QCA, quantitative coronary angiography.

[a]Improved diagnostic accuracy when MFR <2 was added to summed stress score.

[b]Severe 3-vessel CAD was defined visually as a diameter stenosis of the left main coronary artery ≥50% + proximal or mid-segments of the right coronary artery ≥70%; or, proximal or mid-segments of the right coronary artery, left anterior descending artery, and left circumflex artery ≥70% stenosis.

[c]Calculated as the mean MFR of the two lowest scoring segments for each vascular territory.

[d]High-risk CAD on angiography was defined as 2-vessel disease (≥70% stenosis), including the proximal left anterior descending artery; 3-vessel disease; or left main CAD (≥50% stenosis).

1.44–2.5) (Tables 2 and 3). For ^{15}O-water, a regional hyperaemic MBF <2.3 ml/g/min and a regional MFR <2.5 have been shown to identify FFR-based obstructive CAD with high sensitivity and specificity, both at patient- and vessel-level (Danad et al., 2017; Danad et al., 2014) (Tables 2 and 3). For ^{13}N-ammonia, a vascular territory hyperaemic MBF <2 ml/g/min and a vascular territory MFR <2.1 identified FFR-based obstructive CAD at vessel-level (Lee et al., 2016), but different cut-off values have been found in other studies using anatomical stenosis severity as a reference (Hajjiri et al., 2009; Morton et al., 2012; Naya et al., 2014) (Tables 2 and 3). For ^{82}Rb, studies have mainly focused on global MFR showing that 3-vessel CAD is rare in the presence of preserved (>2.0) global MFR (Naya et al., 2014; Ziadi et al., 2012).

The relatively high diagnostic accuracy of PET MPI can be attributed to several factors. The photon energy of PET tracers is substantially higher than that of SPECT tracers, reducing scatter and non-uniform attenuation. The more routine use of attenuation correction with PET MPI further reduces non-uniform attenuation. Additionally, MBF quantification boosts the diagnostic accuracy of PET MPI (Chen et al., 2019). However, some caveats can compromise the diagnostic performance of PET MPI based on absolute MBF quantification in the detection of obstructive CAD. Detection of obstructive CAD by absolute quantification of MBF is prone to false-positive test results due to coronary microvascular dysfunction or inadequate response to pharmacological stressor (Pelletier-Galarneau et al., 2019). In addition to microvascular dysfunction, other factors, such as coronary plaque geometry (shape, eccentricity and length), collateral blood flow and the presence of diffuse coronary atherosclerosis may alter the haemodynamic impact of an epicardial stenosis, particularly in the presence of an intermediate-severity stenosis (Di Carli et al., 1995; Murthy et al., 2018). Overall, quantified MBF has shown better agreement with FFR than anatomical severity of the stenosis. Patient motion is a technical issue that can cause spillover from adjacent structures, leading to erroneous quantification of MBF (Hunter et al., 2016). Similarly, inaccurate timing of tracer injection relative to pharmacological stressor administration may fail to coincide with peak hyperaemia (Johnson & Gould, 2015).

9 | PROGNOSTIC VALUE OF PET MPI

Conventional semi-quantitative ^{82}Rb PET provided incremental prognostic information for predicting adverse cardiac outcome, over clinical risk factors and left ventricular ejection fraction (Dorbala et al., 2013; Dorbala et al., 2009; Yoshinaga et al., 2006). In the largest published study (n = 7061), the magnitude of myocardial ischemia and scar on PET provided significant reclassification of risk in 12% of patients with known or suspected CAD referred for PET MPI for clinical indications (Dorbala et al., 2013).

Tables 4 and 5 summarize the available evidence on the prognostic value of quantitative PET MPI parameters for prediction of adverse outcome at long-term follow-up. Robust evidence (mainly from ^{82}Rb and ^{13}N-ammonia studies) supports incremental prognostic value of global MFR (generally at a cut-off value of 2) over conventional risk predictors, for predicting adverse cardiac outcome at intermediate/long-term follow-up (Bom et al., 2020; Farhad et al., 2013; Fukushima et al., 2011; Gupta et al., 2017; Herzog et al., 2009; Murthy et al., 2011; Slart et al., 2011; Tio et al., 2009; Ziadi et al., 2011). Yet, a recent meta-analysis reported considerable heterogeneity among these studies in predictor operationalization, covariate structure of adopted models, as well as predicted outcome, and follow-up length (Juárez-Orozco et al., 2018). Three of these studies further demonstrated stratification of patient risk using the novel metrics of risk reclassification (net reclassification index, integrated discrimination index) (Gupta et al., 2017; Murthy et al., 2011; Ziadi et al., 2011). Of these, the study with the largest cohort (n = 4029) showed that MFR reclassified 48% of the patients for the risk of cardiovascular death, over a model of clinical risk predictors, semi-quantitative MPI measures and left ventricular ejection fraction (Gupta et al., 2017). Multiple studies have shown that the predictive value of global MFR is maintained regardless of the presence of relative perfusion defects by semi-quantitative PET MPI, or the extent/severity of epicardial CAD by ICA (Gupta et al., 2017; Herzog et al., 2009; Murthy et al., 2011; Taqueti et al., 2015; Ziadi et al., 2011). Moreover, observational data suggest that quantitative PET parameters (MFR and coronary flow capacity derived from both hyperaemic MBF and MFR) may identify patients who prognostically benefit from early revascularization (Gould et al., 2019; Patel et al., 2020; Taqueti et al., 2015). In the largest of these studies (n = 12 594), patients with MFR ≤1.8 derived survival benefit from early revascularization over medical treatment regardless of the type of revascularization, and similar trend was observed within different semi-quantitative levels of ischemia (Patel et al., 2020).

On the other hand, evidence is less consistent for an independent prognostic value of hyperaemic MBF (Bom et al., 2020; Farhad et al., 2013; Fukushima et al., 2011; Gupta et al., 2017; Maaniitty et al., 2017; Murthy et al., 2011). MBF calculation requires estimation of arterial input function and a model to correct for the non-linear first-pass extraction of tracer, particularly in the case of ^{82}Rb. The prognostic value of hyperaemic MBF was variable depending on input function derivation method and extraction model, whereas that of MFR was substantially more consistent and independent on input function method or extraction model (Murthy et al., 2014). Modest evidence (from two studies utilizing ^{15}O-water tracer) exists on the prognostic value of regional hyperaemic MBF and MFR (Bom et al., 2020; Maaniitty et al., 2017). Recently, Bom et al. reported adequate prognostic performance of both global and regional quantitative parameters (hyperaemic MBF and MFR) for predicting hard events; however, the combination of global and regional perfusion did not improve the prognostic performance compared with either alone (Bom et al., 2020).

10 | FUTURE DIRECTIONS

The promising role of the novel tracer ^{18}F-flurpiridaz has been highlighted in the first phase III trial, with greater sensitivity for

TABLE 4 Characteristics of studies which explored the prognostic value of hyperemic MBF

Study	Year	Cohort size	Age (years)	Men (%)	Selection criterion	Tracer	Stressor	Predictor	Primary outcome	Mean FU (months)	HR	(95% CI)	*p* value	Primary outcome events
Fukushima et al.	2011	224	58	38.4	Known or Suspected CAD	^{82}Rb	Dipyridamole	Global hyperemic MBF <1.9	MACE	12	NA	NA	0.09	Cardiac death/ MI/ICA ± PCI/ hospitalization for HF
Murthy et al.	2011	2783	64.8	47.9	Known or Suspected CAD	^{82}Rb	Adenosine/ Dipyridamole/ regadenoson/ dobutamine	Unit decrease in global hyperemic MBF	Cardiac death	16.8	1.1	1.0–1.3	0.07	Cardiac death
Farhad et al.	2013	318	65	63.5	Known or Suspected CAD	^{82}Rb	Adenosine	Unit decrease in global hyperemic MBF[a]	MACE	20.8	2.44	1.49–4.00	0.007	Cardiac death/MI/ revascularization/ hospitalization for HF or SCAD
Gupta et al.	2017	4029	66	49.5	Known or Suspected CAD	^{82}Rb or ^{13} N-ammonia	Adenosine/ Dipyridamole/ regadenoson/ dobutamine	Unit decrease in global hyperemic MBF	Cardiovascular death	117	1.03	0.84–1.27	0.8	Cardiovascular death
Maaniitty et al	2017	864	64	56.5	Suspected CAD	^{15}O-water	Adenosine	Hyperemic MBF ≤2.4 in ≥1 segment	Adverse events	43.2	3.62	1.08 – 12.15	0.04	All-cause death/ MI/UAP
Bom et al.	2020	648	59	54.5	Known or Suspected CAD	^{15}O-water	Adenosine	Global hyperemic MBF <2.65 regional hyperemic MBF[b] <2.1	MACE	82.8	3.03 2.80	1.61–5.70 1.49–5.25	0.001 0.006	All-cause death/MI
Harjulahti et al.	2021	530	65	50.9	Suspected CAD	^{15}O-water	Adenosine	Global hyperemic MBF <2.2 regionalhyperemic MBF ≤2.3 in ≥1 segment	Adverse events	48	3.19 4.59	1.52-6.71 1.59-13.22	0.002 0.005	Cardiovascular death/MI/UAP

Abbreviations: CAD, coronary artery disease; CI, confidence interval; FU, follow-up; HF, heart failure; HR, hazard ratio; ICA, invasive coronary angiography; MACE, major adverse cardiac events; MBF, myocardial blood flow; MI, myocardial infarction; NA, not available; PCI, percutaneous coronary intervention; SCAD, stable coronary artery disease; UAP, unstable angina pectoris.

[a]Global MFR was also included in the multivariable model.

[b]Regional hyperemic MBF values were calculated per vascular territory by averaging the perfusion values of the two adjacent segments with the lowest values.

TABLE 5 Characteristics of studies which explored the prognostic value of MFR

Study	Year	Cohort size	Age (years)	Men (%)	Selection criterion	Tracer	Stressor	Predictor	Primary outcome	Mean FU (months)	HR	(95% CI)	*p* value	Primary outcome events
Tio et al.	2009	344	66	78.8	Known CAD	^{13}N-ammonia	Dipyridamole	SD decrease in global MFR	Cardiac death	85	4.11	2.98–5.67	<0.001	Cardiac death
Herzog et al.	2009	229	60	69	Known or Suspected CAD	^{13}N-ammonia	Adenosine	Global MFR <2	Cardiac death	66	2.86	1.24–6.59	<0.05	Cardiac death
Ziadi et al.	2011	677	64	61.4	Known or Suspected CAD	^{82}Rb	Dipyridamole	Global MFR <2	Cardiac death/ MI	12.9	3.3	1.13–9.5	0.02	Cardiac death/MI
Slart et al.	2011	119	67	80.7	Known CAD	^{13}N-ammonia	Dipyridamole	Unit decrease in global MFR	Cardiac death	88	1.27	1.12–1.43	<0.001	Cardiac death
Fukushima et al.	2011	224	58	38.4	Known or Suspected CAD	^{82}Rb	Dipyridamole	Global MFR <2.11	MACE	12	2.93	1.30–6.65	0.009	Cardiac death/ MI/ICA ± PCI/ hospitalization for HF
Murthy et al.	2011	2783	64.8	47.9	Known or Suspected CAD	^{82}Rb	Adenosine/ Dipyridamole/ regadenoson/ dobutamine	Global MFR lowest tertile[a] global MFR middle tertile[a]	Cardiac death	16.8	5.6 3.4	2.5–12.4 1.5–7.7	<0.001 0.003	Cardiac death
Farhad et al.	2013	318	65	63.5	Known or Suspected CAD	^{82}Rb	Adenosine	Unit decrease in global MFR[b]	MACE	20.8	2.38	NA	0.006	Cardiac death/MI/ revascularization/ hospitalization for HF or SCAD
Gupta et al.	2017	4029	66	49.5	Known or Suspected CAD	^{82}Rb or ^{13}N-ammonia	Adenosine/ Dipyridamole/ regadenoson/ Dobutamine	Unit decrease in global MFR	Cardiovascular death	117	1.83	1.47–2.27	<0.001	Cardiovascular death
Bom et al.	2020	648	59	54.5	Known or Suspected CAD	^{15}O-water	Adenosine	Global MFR <2.88 regional MFR[c] <2.07	MACE	82.8	2.12 2.33	1.15–3.90 1.30–4.18	0.016 0.005	All-cause death/MI

Abbreviations: CAD, coronary artery disease; CI, confidence interval; FU, follow-up; HF, heart failure; HR, hazard ratio; ICA, invasive coronary angiography; MACE, major adverse cardiac events; MFR, myocardial flow reserve; MI, myocardial infarction; NA, not available; PCI, percutaneous coronary intervention; SCAD, stable coronary artery disease; SD, standard deviation.

[a]Compared with the highest tertile of global MFR.

[b]Global hyperemic MBF was not included in the multivariable model.

[c]Regional hyperemic MBF values were calculated per vascular territory by averaging the perfusion values of the two adjacent segments with the lowest values.

detection of CAD using visual analysis (50% stenosis or documented prior myocardial infarction) compared with SPECT, in addition to superior image quality, higher diagnostic certainty, and lower radiation dose; however, it failed to achieve superiority in specificity (Maddahi et al., 2020). Another phase III trial is underway (NLM identifier: NCT03354273). Standardization of software used for analysis of MBF is still needed among the commercially available software products, particularly those adapted for different tracers (Dekemp et al., 2013; Nesterov et al., 2014; Slomka et al., 2012; Tahari et al., 2014). Additionally, the recent stressor regadenoson was highly effective for detection of CAD and showed lower atrioventricular block rates compared with adenosine (Andrikopoulou et al., 2019; Hsiao et al., 2013). Furthermore, a simple stress-only protocol could be adequate for detection of CAD (Danad et al., 2014; Hajjiri et al., 2009; Joutsiniemi et al., 2014; Kajander et al., 2011).

In addition to patients with suspected obstructive CAD, quantification of MBF by PET has been applied in other conditions. PET MPI has shown high diagnostic accuracy for the detection of cardiac allograft vasculopathy after heart transplantation, especially when quantitative PET parameters were employed (Bravo et al., 2018; Chih et al., 2018). Moreover, MBF was predictive of major adverse cardiac events at a median follow-up of 2.3 years in this patient group (Bravo et al., 2018). Abnormal MFR is common finding in cardiomyopathies and heart failure due to various aetiologies (Cecchi et al., 2003; Neglia et al., 2002; Taqueti et al., 2018) even in the absence of obstructive epicardial CAD. Normal MFR can rule out severe multi-vessel CAD in patients with reduced left ventricular systolic function (Naya et al., 2014; Ziadi et al., 2012). Furthermore, impaired MFR is associated with major adverse events in patients with both ischaemic and non-ischaemic aetiology of cardiomyopathy (Benz et al., 2021a, 2021b; Majmudar et al., 2015).

In the presence of ischaemic left ventricular dysfunction and resting myocardial perfusion abnormalities, assessment of myocardial glucose metabolism with ^{18}F-fluorodeoxyglucose (^{18}F-FDG) PET enables sensitive detection of viable myocardium with potential for improvement of contractile function upon revascularization (Madsen et al., 2020). Based on retrospective cohort of patients with left ventricular systolic dysfunction undergoing rest–stress ^{82}Rb PET MPI and ^{18}F-FDG PET, the presence of hibernating myocardium was particularly predictive of clinical benefit from revascularization (Ling et al., 2013). Compared with ^{18}F-FDG, resting myocardial perfusion PET alone has inferior accuracy for differentiation between viable and infarcted myocardium (Benz et al., 2021a, 2021b; Grönman et al., 2019; Moody et al., 2019), but nitrate administration has been shown to increase MBF in viable myocardium, leading to improved assessment of viability (Slart et al., 2006).

Further evidence is needed to establish the prognostic role of ^{15}O-water PET, hyperaemic MBF, and relative impact of regional vs. global quantitative PET MPI parameters. Finally, randomized trials are awaited to support the triage of patients for cardiac catheterization and possible revascularization based on PET MPI quantitative measures.

11 | CONCLUSIONS

Assessment of myocardial ischaemia by PET is an accurate tool to detect obstructive CAD. Accumulating evidence indicates that PET perfusion imaging provides prognostic information similar to SPECT imaging. Quantification of absolute MBF and MFR may be helpful in identification of patients with extensive CAD and provide incremental risk stratification over regional ischaemia and clinical information.

ACKNOWLEDGEMENTS

This work has been supported by grants from the Academy of Finland, Finnish Foundation for Cardiovascular Research and by State Research Funding from the Hospital District of Southwest Finland.

CONFLICT OF INTEREST

Dr. Knuuti reports being at speaker bureau at GE Healthcare, Merck, Lundbeck and Bayer and recipient of consultancy fees from GE Healthcare and AstraZeneca. Dr. Saraste reports fees for lectures from Abbott, Amgen, Astra Zeneca, Bayer and Novartis and fees for consultancy from Amgen and Astra Zenaca. Dr. Maaniitty and Dr. Nammas report no relationship with industry.

ORCID

Antti Saraste https://orcid.org/0000-0003-2488-0893

REFERENCES

Al-Mallah, M.H., Sitek, A., Moore, S.C., Di Carli, M. & Dorbala, S. (2010) Assessment of myocardial perfusion and function with PET and PET/CT. *Journal of Nuclear Cardiology*, *17*, 498–513.

Anagnostopoulos, C., Almonacid, A., El Fakhri, G., Curillova, Z., Sitek, A. & Roughton, M. (2008) Quantitative relationship between coronary vasodilator reserve assessed by 82-Rb PET imaging and coronary artery stenosis severity. *European Journal of Nuclear Medicine and Molecular Imaging*, *35*, 1593–1601.

Andrikopoulou, E., Morgan, C.J., Brice, L., Bajaj, N.S., Doppalapudi, H., Iskandrian, A.E. et al. (2019) Incidence of atrioventricular block with vasodilator stress SPECT: a meta-analysis. *Journal of Nuclear Cardiology*, *26*, 616–628.

Bartunek, J., Wijns, W., Heyndrickx, G.R. & de Bruyne, B. (1999) Effects of dobutamine on coronary stenosis physiology and morphology: comparison with intracoronary adenosine. *Circulation*, *100*, 243–249.

Benz, D.C., Ferro, P., Safa, N., Messerli, M., von Felten, E., Huang, W. et al. (2021) Role of quantitative myocardial blood flow and (13)N-ammonia washout for viability assessment in ischemic cardiomyopathy. *Journal of Nuclear Cardiology*, *28*, 263–273.

Benz, D.C., Kaufmann, P.A., von Felten, E., Benetos, G., Rampidis, G., Messerli, M. et al. (2021) Prognostic value of quantitative metrics from positron emission tomography in ischemic heart failure. *JACC: Cardiovascular Imaging*, *14*, 454–464.

Berman, D.S., Kang, X., Slomka, P.J., Gerlach, J., de Yang, L., Hayes, S.W. et al. (2007) Underestimation of extent of ischemia by gated SPECT myocardial perfusion imaging in patients with left main coronary artery disease. *Journal of Nuclear Cardiology*, *14*, 521–528.

Berman, D.S., Maddahi, J., Tamarappoo, B.K., Czernin, J., Taillefer, R., Udelson, J.E. et al. (2013) Phase II safety and clinical comparison with single-photon emission computed tomography myocardial perfusion imaging for detection of coronary artery disease: flurpiridaz F

18 positron emission tomography. *Journal of the American College of Cardiology*, *61*, 469–477.

Bom, M.J., van Diemen, P.A., Driessen, R.S., Everaars, H., Schumacher, S.P., Wijmenga, J.T. et al. (2020) Prognostic value of [15O]H2O positron emission tomography-derived global and regional myocardial perfusion. *European Heart Journal of Cardiovascular Imaging*, *21*, 777–786.

Bravo, P.E., Bergmark, B.A., Vita, T., Taqueti, V.R., Gupta, A., Seidelmann, S. et al. (2018) Diagnostic and prognostic value of myocardial blood flow quantification as non-invasive indicator of cardiac allograft vasculopathy. *European Heart Journal*, *39*, 316–323.

Brown, B.G., Josephson, M.A., Petersen, R.B., Pierce, C.D., Wong, M., Hecht, H.S. et al. (1981) Intravenous dipyridamole combined with isometric handgrip for near maximal acute increase in coronary flow in patients with coronary artery disease. *American Journal of Cardiology*, *48*, 1077–1085.

Cecchi, F., Olivotto, I., Gistri, R., Lorenzoni, R., Chiriatti, G. & Camici, P.G. (2003) Coronary microvascular dysfunction and prognosis in hypertrophic cardiomyopathy. *New England Journal of Medicine*, *349*, 1027–1035.

Chen, K., Miller, E.J. & Sadeghi, M.M. (2019) PET-based imaging of ischemic heart disease. *PET Clinics*, *14*, 211–221.

Chih, S., Chong, A.Y., Erthal, F., deKemp, R.A., Davies, R.A., Stadnick, E. et al. (2018) PET Assessment of epicardial intimal disease and microvascular dysfunction in cardiac allograft vasculopathy. *Journal of the American College of Cardiology*, *71*, 1444–1456.

Chow, B.J., Beanlands, R.S., Lee, A., DaSilva, J.N., deKemp, R.A., Alkahtani, A. et al. (2006) Treadmill exercise produces larger perfusion defects than dipyridamole stress N-13 ammonia positron emission tomography. *Journal of the American College of Cardiology*, *47*, 411–416.

Czernin, J., Auerbach, M., Sun, K.T., Phelps, M. & Schelbert, H.R. (1995) Effects of modified pharmacologic stress approaches on hyperemic myocardial blood flow. *Journal of Nuclear Medicine*, *36*, 575–580.

Danad, I., Raijmakers, P.G., Appelman, Y.E., Harms, H.J., de Haan, S., van den Oever, M.L. et al. (2013) Hybrid imaging using quantitative H215O PET and CT-based coronary angiography for the detection of coronary artery disease. *Journal of Nuclear Medicine*, *54*, 55–63.

Danad, I., Raijmakers, P.G., Driessen, R.S., Leipsic, J., Raju, R., Naoum, C. et al. (2017) Comparison of coronary CT angiography, SPECT, PET, and hybrid imaging for diagnosis of ischemic heart disease determined by fractional flow reserve. *JAMA Cardiology*, *2*, 1100–1107.

Danad, I., Uusitalo, V., Kero, T., Saraste, A., Raijmakers, P.G., Lammertsma, A.A. et al. (2014) Quantitative assessment of myocardial perfusion in the detection of significant coronary artery disease: cutoff values and diagnostic accuracy of quantitative [15O]H2O PET imaging. *Journal of the American College of Cardiology*, *64*, 1464–1475.

De Grado, T.R., Hanson, M., Turkington, T., Delong, D., Brezinski, D. & Vallee, J. (1996) Estimation of myocardial blood flow for longitudinal studies with 13N-labeled ammonia and positron emission tomography. *Journal of Nuclear Cardiology*, *3*, 494–507.

Dekemp, R.A., Declerck, J., Klein, R., Pan, X.B., Nakazato, R., Tonge, C. et al. (2013) Multisoftware reproducibility study of stress and rest myocardial blood flow assessed with 3D dynamic PET/CT and a 1-tissue-compartment model of 82Rb kinetics. *Journal of Nuclear Medicine*, *54*, 571–577.

Di Carli, M., Czernin, J., Hoh, C.K., Gerbaudo, V.H., Brunken, R.C., Huang, S.C. et al. (1995) Relation among stenosis severity, myocardial blood flow, and flow reserve in patients with coronary artery disease. *Circulation*, *91*, 1944–1951.

Dorbala, S., Di Carli, M.F., Beanlands, R.S., Merhige, M.E., Williams, B.A., Veledar, E. et al. (2013) Prognostic value of stress myocardial perfusion positron emission tomography: results from a multicenter observational registry. *Journal of the American College of Cardiology*, *61*, 176–184.

Dorbala, S., Hachamovitch, R., Curillova, Z., Thomas, D., Vangala, D., Kwong, R.Y. et al. (2009) Incremental prognostic value of gated Rb-82 positron emission tomography myocardial perfusion imaging over clinical variables and rest LVEF. *JACC: Cardiovascular Imaging*, *2*, 846–854.

El Fakhri, G., Kardan, A., Sitek, A., Dorbala, S., Abi-Hatem, N., Lahoud, Y. et al. (2009) Reproducibility and accuracy of quantitative myocardial blood flow assessment with (82)Rb PET: comparison with (13) Nammonia PET. *Journal of Nuclear Medicine*, *50*, 1062–1071.

Farhad, H., Dunet, V., Bachelard, K., Allenbach, G., Kaufmann, P.A. & Prior, J.O. (2013) Added prognostic value of myocardial blood flow quantitation in rubidium-82 positron emission tomography imaging. *European Heart Journal of Cardiovascular Imaging*, *14*, 1203–1210.

Fiechter, M., Ghadri, J.R., Gebhard, C., Fuchs, T.A., Pazhenkottil, A.P., Nkoulou, R.N. et al. (2012) Diagnostic value of 13N-ammonia myocardial perfusion PET: added value of myocardial flow reserve. *Journal of Nuclear Medicine*, *53*, 1230–1234.

Fukushima, K., Javadi, M.S., Higuchi, T., Lautamaki, R., Merrill, J., Nekolla, S.G. & Bengel, F.M. (2011) Prediction of short-term cardiovascular events using quantification of global myocardial flow reserve in patients referred for clinical 82Rb PET perfusion imaging. *Journal of Nuclear Medicine*, *52*, 726–732.

Gewirtz, H. (2019) Coronary circulation: pressure/flow parameters for assessment of ischemic heart disease. *Journal of Nuclear Cardiology*, *26*, 459–470.

Gould, K.L., Johnson, N.P., Roby, A.E., Nguyen, T., Kirkeeide, R., Haynie, M. et al. (2019) Regional, artery-specific thresholds of quantitative myocardial perfusion by PET associated with reduced myocardial infarction and death after revascularization in stable coronary artery disease. *Journal of Nuclear Medicine*, *60*, 410–417.

Gould, K.L., Kirkeeide, R.L. & Buchi, M. (1990) Coronary flow reserve as a physiologic measure of stenosis severity. *Journal of the American College of Cardiology*, *15*, 459–474.

Gould, K.L., Pan, T., Loghin, C., Johnson, N.P., Guha, A. & Sdringola, S. (2007) Frequent diagnostic errors in cardiac PET/CT due to misregistration of CT attenuation and emission PET images: a definitive analysis of causes, consequences, and corrections. *Journal of Nuclear Medicine*, *48*, 1112–1121.

Grönman, M., Tarkia, M., Stark, C., Vähäsilta, T., Kiviniemi, T., Lubberink, M., Halonen, P., Kuivanen, A., Saunavaara, V., Tolvanen, T., Teuho, J., Teräs, M., Savunen, T., Pietilä, M., Ylä-Herttuala, S., Roivainen, A., Knuuti, J. & Saraste, A. (2019) Assessment of myocardial viability with [15O]water PET: a validation study in experimental myocardial infarction. *Journal of Nuclear Cardiology*. In press.

Guehl, N.J., Normandin, M.D., Wooten, D.W., Rozen, G., Sitek, A., Ruskin, J. et al. (2017) Single-scan rest/stress imaging: validation in a porcine model with (18)F-Flurpiridaz. *European Journal of Nuclear Medicine and Molecular Imaging*, *44*, 1538–1546.

Gupta, A., Taqueti, V.R., van de Hoef, T.P., Bajaj, N.S., Bravo, P.E., Murthy, V.L. et al. (2017) Integrated non-invasive physiological assessment of coronary circulatory function and impact on cardiovascular mortality in patients with stable coronary artery disease. *Circulation*, *136*, 2325–2336.

Hajjiri, M.M., Leavitt, M.B., Zheng, H., Spooner, A.E., Fischman, A.J. & Gewirtz, H. (2009) Comparison of positron emission tomography measurement of adenosine-stimulated absolute myocardial blood flow versus relative myocardial tracer content for physiological assessment of coronary artery stenosis severity and location. *JACC: Cardiovascular Imaging*, *2*, 751–758.

Harjulahti, E., Maaniitty, T., Nammas, W., Stenström, I., Biancari, F., & Bax, J.J. et al. (2021) Global and segmental absolute stress myocardial blood flow in prediction of cardiac events: 15O-water positron emission tomography study. *European Journal of Nuclear Medicine and Molecular Imaging*, *48*, 1434–1444. https://doi.org/10.1007/s00259-020-05093-2

Harms, H.J., Knaapen, P., de Haan, S., Halbmeijer, R., Lammertsma, A.A. & Lubberink, M. (2011) Automatic generation of absolute myocardial blood flow images using [15O]H2O and a clinical PET/CT scanner. *European Journal of Nuclear Medicine and Molecular Imaging*, *38*, 930–939.

Herzog, B.A., Husmann, L., Valenta, I., Gaemperli, O., Siegrist, P.T., Tay, F.M. et al. (2009) Long-term prognostic value of ^{13}N-ammonia myocardial perfusion positron emission tomography added value of coronary flow reserve. *Journal of the American College of Cardiology*, *54*, 150–156.

Higuchi, T., Nekolla, S.G., Huisman, M.M., Reder, S., Poethko, T., Yu, M. et al. (2008) A new 18F-labeled myocardial PET tracer: myocardial uptake after permanent and transient coronary occlusion in rats. *Journal of Nuclear Medicine*, *49*, 1715–1722.

Hsiao, E., Ali, B., Blankstein, R., Skali, H., Ali, T., Bruyere, J. Jr et al. (2013) Detection of obstructive coronary artery disease using regadenoson stress and 82Rb PET/CT myocardial perfusion imaging. *Journal of Nuclear Medicine*, *54*, 1748–1754.

Huisman, M.C., Higuchi, T., Reder, S., Nekolla, S.G., Poethko, T., Wester, H.J. et al. (2008) Initial characterization of an 18F-labeled myocardial perfusion tracer. *Journal of Nuclear Medicine*, *49*, 630–636.

Hunter, C.R.R.N., Klein, R., Beanlands, R.S. & deKemp, R.A. (2016) Patient motion effects on the quantification of regional myocardial blood flow with dynamic PET imaging. *Medical Physics*, *43*, 1829.

Hutchins, G.D., Schwaiger, M., Rosenspire, K.C., Krivokapich, J., Schelbert, H. & Kuhl, D.E. (1990) Noninvasive quantification of regional blood flow in the human heart using N-13 ammonia and dynamic positron emission tomographic imaging. *Journal of the American College of Cardiology*, *15*, 1032–1042.

Iida, H., Kanno, I., Takahashi, A., Miura, S., Murakami, M., Takahashi, K. et al. (1988) Measurement of absolute myocardial blood flow with H2 15O and dynamic positron-emission tomography. Strategy for quantification in relation to the partial-volume effect. *Circulation*, *78*, 104–115.

Jaarsma, C., Leiner, T., Bekkers, S.C., Crijns, H.J., Wildberger, J.E., Nagel, E. et al. (2012) Diagnostic performance of noninvasive myocardial perfusion imaging using single-photon emission computed tomography, cardiac magnetic resonance, and positron emission tomography imaging for the detection of obstructive coronary artery disease: a meta-analysis. *Journal of the American College of Cardiology*, *59*, 1719–1728.

Johnson, N.P. & Gould, K.L. (2011) Physiological basis for angina and ST-segment change: PET-verified thresholds of quantitative stress myocardial perfusion and coronary flow reserve. *JACC: Cardiovascular Imaging*, *4*, 990–998.

Johnson, N.P. & Gould, K.L. (2015) Regadenoson versus dipyridamole hyperemia for cardiac PET imaging. *JACC: Cardiovascular Imaging*, *8*, 438–447.

Joutsiniemi, E., Saraste, A., Pietilä, M., Mäki, M., Kajander, S., Ukkonen, H. et al. (2014) Absolute flow or myocardial flow reserve for the detection of significant coronary artery disease? *European Heart Journal of Cardiovascular Imaging*, *15*, 659–665.

Juárez-Orozco, L.E., Tio, R.A., Alexanderson, E., Dweck, M., Vliegenthart, R., El Moumni, M. et al. (2018) Quantitative myocardial perfusion evaluation with positron emission tomography and the risk of cardiovascular events in patients with coronary artery disease: a systematic review of prognostic studies. *European Heart Journal of Cardiovascular Imaging*, *19*, 1179–1187.

Kajander, S., Joutsiniemi, E., Saraste, M., Pietilä, M., Ukkonen, H., Saraste, A. et al. (2010) Cardiac positron emission tomography/computed tomography imaging accurately detects anatomically and functionally significant coronary artery disease. *Circulation*, *122*, 603–613.

Kajander, S.A., Joutsiniemi, E., Saraste, M., Pietilä, M., Ukkonen, H., Saraste, A. et al. (2011) Clinical value of absolute quantification of myocardial perfusion with (15)O-water in coronary artery disease. *Circulation: Cardiovascular Imaging*, *4*, 678–684.

Keiding, S., Sørensen, M., Munk, O.L. & Bender, D. (2010) Human 13N-ammonia PET studies: the importance of measuring 13N-ammonia metabolites in blood. *Metabolic Brain Disease*, *25*, 49–56.

Klein, R., Ocneanu, A., Renaud, J.M., Ziadi, M.C., Beanlands, R.S.B. & deKemp, R.A. (2018) Consistent tracer administration profile improves test-retest repeatability of myocardial blood flow quantification with 82Rb dynamic PET imaging. *Journal of Nuclear Cardiology*, *25*, 929–941.

Knuuti, J., Ballo, H., Juarez-Orozco, L.E., Saraste, A., Kolh, P., Rutjes, A.W.S. et al. (2018) The performance of non-invasive tests to rule-in and rule-out significant coronary artery stenosis in patients with stable angina: a meta-analysis focused on post-test disease probability. *European Heart Journal*, *39*, 3322–3330.

Knuuti, J. & Saraste, A. (2012) Advances in clinical application of quantitative myocardial perfusion imaging. *Journal of Nuclear Cardiology*, *19*, 643–646.

Knuuti, J., Wijns, W., Saraste, A., Capodanno, D., Barbato, E., Funck-Brentano, C. et al. (2020) 2019 ESC Guidelines for the diagnosis and management of chronic coronary syndromes. *European Heart Journal*, *41*, 407–477.

Krivokapich, J., Huang, S.C., Phelps, M.E., MacDonald, N.S. & Shine, K.I. (1982) Dependence of ^{13}NH3 myocardial extraction and clearance on flow and metabolism. *American Journal of Physiology*, *242*, H536–H542.

Krivokapich, J., Smith, G.T., Huang, S.C., Hoffman, E.J., Ratib, O., Phelps, M.E. et al. (1989) 13N ammonia myocardial imaging at rest and with exercise in normal volunteers. Quantification of absolute myocardial perfusion with dynamic positron emission tomography. *Circulation*, *80*, 1328–1337.

Lapeyre, A.C., Goraya, T.Y., Johnston, D.L. & Gibbons, R.J. (2004) The impact of caffeine on vasodilator stress perfusion studies. *Journal of Nuclear Cardiology*, *11*, 506–511.

Lautamäki, R., George, R.T., Kitagawa, K., Higuchi, T., Merrill, J., Voicu, C. et al. (2009) Rubidium-82 PET-CT for quantitative assessment of myocardial blood flow: Validation in a canine model of coronary artery stenosis. *European Journal of Nuclear Medicine and Molecular Imaging*, *36*, 576–586.

Lee, J.M., Kim, C.H., Koo, B.-K., Hwang, D., Park, J., Zhang, J. et al. (2016) Integrated myocardial perfusion imaging diagnostics improve detection of functionally significant coronary artery stenosis by 13Nammonia positron emission tomography. *Circulation: Cardiovascular Imaging*, *9*, e004768.

Ling, L.F., Marwick, T.H., Flores, D.R., Jaber, W.A., Brunken, R.C., Cerqueira, M.D. et al. (2013) Identification of therapeutic benefit from revascularization in patients with left ventricular systolic dysfunction: inducible ischemia versus hibernating myocardium. *Circulation: Cardiovascular Imaging*, *6*, 363–372.

Lortie, M., Beanlands, R.S., Yoshinaga, K., Klein, R., Dasilva, J.N. & DeKemp, R.A. (2007) Quantification of myocardial blood flow with 82-Rb dynamic PET imaging. *European Journal of Nuclear Medicine and Molecular Imaging*, *34*, 1765–1774.

Maaniitty, T., Stenström, I., Bax, J.J., Uusitalo, V., Ukkonen, H., Kajander, S. et al. (2017) Prognostic value of coronary CT angiography with selective PET perfusion imaging in coronary artery disease. *JACC: Cardiovascular Imaging*, *10*, 1361–1370.

Maddahi, J., Bengel, F., Czernin, J., Crane, P., Dahlbom, M., Schelbert, H. et al. (2019) Dosimetry, biodistribution, and safety of flurpiridaz F 18 in healthy subjects undergoing rest and exercise or pharmacological stress PET myocardial perfusion imaging. *Journal of Nuclear Cardiology*, *26*, 2018–2030.

Maddahi, J., Bengel, F., Huang, S.C., Czernin, J., Schelbert, H., Zhu, Q. et al. (2009) Phase 1 rest-stress study of F-18 labeled BMS747158 myocardial perfusion PET tracer: human safety, dosimetry,

biodistribution, and myocardial imaging characteristics. *Journal of Nuclear Medicine*, *50*, 184. abstract.

Maddahi, J., Czernin, J., Lazewatsky, J., Huang, S.C., Dahlbom, M., Schelbert, H. et al. (2011) Phase I, first-in-human study of BMS747158, a novel 18F-labeled tracer for myocardial perfusion PET: dosimetry, biodistribution, safety, and imaging characteristics after a single injection at rest. *Journal of Nuclear Medicine*, *52*, 1490–1498.

Maddahi, J., Lazewatsky, J., Udelson, J.E., Berman, D.S., Beanlands, R.S.B., Heller, G.V. et al. (2020) Phase-III clinical trial of fluorine-18 flurpiridaz positron emission tomography for evaluation of coronary artery disease. *Journal of the American College of Cardiology*, *76*, 391–401.

Maddahi, J. & Packard, R.R. (2014) Cardiac PET perfusion tracers: current status and future directions. *Seminars in Nuclear Medicine*, *44*, 333–343.

Madsen, S., Dias, A.H., Lauritsen, K.M., Bouchelouche, K., Tolbod, L.P. & Gormsen, L.C. (2020) Myocardial viability testing by positron emission tomography: basic concepts, mini-review of the literature and experience from a tertiary PET center. *Seminars in Nuclear Medicine*, *50*, 248–259.

Majmudar, M.D., Murthy, V.L., Shah, R.V., Kolli, S., Mousavi, N., Foster, C.R. et al. (2015) Quantification of coronary flow reserve in patients with ischaemic and non-ischaemic cardiomyopathy and its association with clinical outcomes. *European Heart Journal of Cardiovascular Imaging*, *16*, 900–909.

Mc Ardle, B.A., Dowsley, T.F., deKemp, R.A., Wells, G.A. & Beanlands, R.S. (2012) Does rubidium-82 pet have superior accuracy to spect perfusion imaging for the diagnosis of obstructive coronary disease?: a systematic review and meta-analysis. *Journal of the American College of Cardiology*, *60*, 1828–1837.

McGinn, A.L., White, C.W. & Wilson, R.F. (1990) Interstudy variability of coronary flow reserve: influence of heart rate, arterial blood pressure, and ventricular preload. *Circulation*, *81*, 1319–1330.

Moody, J.B., Hiller, K.M., Lee, B.C., Poitrasson-Rivière, A., Corbett, J.R., Weinberg, R.L. et al. (2019) The utility of (82)Rb PET for myocardial viability assessment: comparison with perfusion-metabolism (82)Rb-(18)F-FDG PET. *Journal of Nuclear Cardiology*, *26*, 374–386.

Moody, J.B., Poitrasson-Rivière, A., Hagio, T., Buckley, C., Weinberg, R.L., Corbett, J.R. et al. (2020) Added value of myocardial blood flow using 18F-flurpiridaz PET to diagnose coronary artery disease: the flurpiridaz 301 trial. *Journal of Nuclear Cardiology*. In press.

Morton, G., Chiribiri, A., Ishida, M., Hussain, S.T., Schuster, A., Indermuehle, A. et al. (2012) Quantification of absolute myocardial perfusion in patients with coronary artery disease: comparison between cardiovascular magnetic resonance and positron emission tomography. *Journal of the American College of Cardiology*, *60*, 1546–1555.

Murthy, V.L., Bateman, T.M., Beanlands, R.S., Berman, D.S., Borges-Neto, S., Chareonthaitawee, P. et al. (2018) Clinical quantification of myocardial blood flow using PET: joint position paper of the SNMMI cardiovascular council and the ASNC. *Journal of Nuclear Medicine*, *59*, 273–293.

Murthy, V.L., Lee, B.C., Sitek, A., Naya, M., Moody, J., Polavarapu, V. et al. (2014) Comparison and prognostic validation of multiple methods of quantification of myocardial blood flow with 82Rb PET. *Journal of Nuclear Medicine*, *55*, 1952–1958.

Murthy, V.L., Naya, M., Foster, C.R., Hainer, J., Gaber, M., Di Carli, G. et al. (2011) Improved cardiac risk assessment with noninvasive measures of coronary flow reserve. *Circulation*, *124*, 2215–2224.

Muzik, O., Beanlands, R.S., Hutchins, G.D., Mangner, T.J., Nguyen, N. & Schwaiger, M. (1993) Validation of nitrogen-13-ammonia tracer kinetic model for quantification of myocardial blood flow using PET. *Journal of Nuclear Medicine*, *34*, 83–91.

Naya, M., Murthy, V.L., Taqueti, V.R., Foster, C.R., Klein, J., Garber, M. et al. (2014) Preserved coronary flow reserve effectively excludes high-risk coronary artery disease on angiography. *Journal of Nuclear Medicine*, *55*, 248–255.

Neglia, D., Michelassi, C., Trivieri, M.G., Sambuceti, G., Giorgetti, A., Pratali, L. et al. (2002) Prognostic role of myocardial blood flow impairment in idiopathic left ventricular dysfunction. *Circulation*, *105*, 186–193.

Nekolla, S.G., Reder, S., Saraste, A., Higuchi, T., Dzewas, G., Preissel, A. et al. (2009) Evaluation of the novel myocardial perfusion positron-emission tomography tracer 18F-BMS-747158-02: comparison to 13N-ammonia and validation with microspheres in a pig model. *Circulation*, *119*, 2333–2342.

Nesterov, S.V., Deshayes, E., Sciagrà, R., Settimo, L., Declerck, J.M., Pan, X.B. et al. (2014) Quantification of myocardial blood flow in absolute terms using 82Rb PET imaging: the RUBY-10 study. *JACC: Cardiovascular Imaging*, *11*, 1119–1127.

Packard, R.R., Huang, S.C., Dahlbom, M., Czernin, J. & Maddahi, J. (2014) Absolute quantitation of myocardial blood flow in human subjects with or without myocardial ischemia using dynamic flurpiridaz F 18 PET. *Journal of Nuclear Medicine*, *55*, 1438–1444.

Patel, K.K., Spertus, J.A., Chan, P.S., Sperry, B.W., Al Badarin, F., Kennedy, K.F. et al. (2020) Myocardial blood flow reserve assessed by positron emission tomography myocardial perfusion imaging identifies patients with a survival benefit from early revascularization. *European Heart Journal*, *41*, 759–768.

Pelletier-Galarneau, M., Martineau, P. & El Fakhri, G. (2019) Quantification of PET myocardial blood flow. *Current Cardiology Reports*, *21*, 11.

Rajaram, M., Tahari, A.K., Lee, A.H., Lodge, M.A., Tsui, B., Nekolla, S. et al. (2013) Cardiac PET/CT misregistration causes significant changes in estimated myocardial blood flow. *Journal of Nuclear Medicine*, *54*, 50–54.

Renaud, J.M., Yip, K., Guimond, J., Trottier, M., Pibarot, P., Turcotte, E. et al. (2017) Characterization of 3-dimensional PET systems for accurate quantification of myocardial blood flow. *Journal of Nuclear Medicine*, *58*, 103–109.

Saraste, A., Kajander, S., Han, C., Nesterov, S.V. & Knuuti, J. (2012) PET: is myocardial flow quantification a clinical reality? *Journal of Nuclear Cardiology*, *19*, 1044–1059.

Schindler, T.H., Quercioli, A., Valenta, I., Ambrosio, G., Wahl, R.L. & Dilsizian, V. (2014) Quantitative assessment of myocardial blood flow–clinical and research applications. *Seminars in Nuclear Medicine*, *44*, 274–293.

Sherif, H.M., Nekolla, S.G., Saraste, A., Reder, S., Yu, M., Robinson, S. et al. (2011) Simplified quantification of myocardial flow reserve with flurpiridaz F 18: validation with microspheres in a pig model. *Journal of Nuclear Medicine*, *52*, 617–624.

Sherif, H.M., Saraste, A., Weidl, E., Weber, A.W., Higuchi, T., Reder, S. et al. (2009) Evaluation of a novel (18) F-labeled positron-emission tomography perfusion tracer for the assessment of myocardial infarct size in rats. *Circulation: Cardiovascular Imaging*, *2*, 77–84.

Slart, R.H., Agool, A., van Veldhuisen, D.J., Dierckx, R.A. & Bax, J.J. (2006) Nitrate administration increases blood flow in dysfunctional but viable myocardium, leading to improved assessment of myocardial viability: a PET study. *Journal of Nuclear Medicine*, *47*, 1307–1311.

Slart, R.H.J.A., Zeebregts, C.J., Hillege, H.L., de Sutter, J., Dierckx, R.A.J.O., van Veldhuisen, D.J. et al. (2011) Myocardial perfusion reserve after a PET-driven revascularization procedure: a strong prognostic factor. *Journal of Nuclear Medicine*, *52*, 873–879.

Slomka, P.J., Alexanderson, E., Jácome, R., Jiménez, M., Romero, E., Meave, A. et al. (2012) Comparison of clinical tools for measurements of regional stress and rest myocardial blood flow assessed with 13N-ammonia PET/CT. *Journal of Nuclear Medicine*, *53*, 171–181.

Tadamura, E., Iida, H., Matsumoto, K., Mamede, M., Kubo, S., Toyoda, H. et al. (2001) Comparison of myocardial blood flow during dobutamine-atropine infusion with that after dipyridamole

administration in normal men. *Journal of the American College of Cardiology*, *37*, 130–136.

Tahari, A.K., Lee, A., Rajaram, M., Fukushima, K., Lodge, M.A., Lee, B.C. et al. (2014) Absolute myocardial flow quantification with 82Rb PET/CT: comparison of different software packages and methods. *European Journal of Nuclear Medicine and Molecular Imaging*, *41*, 126–135.

Takx, R.A., Blomberg, B.A., El Aidi, H., Habets, J., de Jong, P.A., Nagel, E. et al. (2015) Diagnostic accuracy of stress myocardial perfusion imaging compared to invasive coronary angiography with fractional flow reserve meta-analysis. *Circulation: Cardiovascular Imaging*, *8*, e002666.

Tamaki, N., Yonekura, Y., Senda, M., Kureshi, S.A., Saji, H., Kodama, S. et al. (1985) Myocardial positron computed tomography with 13N-ammonia at rest and during exercise. *European Journal of Nuclear Medicine*, *11*, 246–251.

Taqueti, V.R., Hachamovitch, R., Murthy, V.L., Naya, M., Foster, C.R., Hainer, J. et al. (2015) Global coronary flow reserve is associated with adverse cardiovascular events independently of luminal angiographic severity and modifies the effect of early revascularization. *Circulation*, *131*, 19–27.

Taqueti, V.R., Solomon, S.D., Shah, A.M., Desai, A.S., Groarke, J.D., Osborne, M.T. et al. (2018) Coronary microvascular dysfunction and future risk of heart failure with preserved ejection fraction. *European Heart Journal*, *39*, 840–849.

Tio, R.A., Dabeshlim, A., Siebelink, H.-M.-J., de Sutter, J., Hillege, H.L., Zeebregts, C.J. et al. (2009) Comparison between the prognostic value of left ventricular function and myocardial perfusion reserve in patients with ischemic heart disease. *Journal of Nuclear Medicine*, *50*, 214–219.

Yalamanchili, P., Wexler, E., Hayes, M., Yu, M., Bozek, J., Kagan, M. et al. (2007) Mechanism of uptake and retention of F-18 BMS-747158-02 in cardiomyocytes: a novel PET myocardial imaging agent. *Journal of Nuclear Cardiology*, *14*, 782–788.

Yoshida, K., Mullani, N. & Gould, K.L. (1996) Coronary flow and flow reserve by PET simplified for clinical applications using rubidium-82 or nitrogen-13-ammonia. *Journal of Nuclear Medicine*, *37*, 1701–1712.

Yoshinaga, K., Chow, B.J., Williams, K., Chen, L., deKemp, R.A., Garrard, L. et al. (2006) What is the prognostic value of myocardial perfusion imaging using rubidium-82 positron emission tomography? *Journal of the American College of Cardiology*, *48*, 1029–1039.

Yu, M., Guaraldi, M.T., Mistry, M., Kagan, M., McDonald, J.L., Drew, K. et al. (2007) BMS-747158-02: a novel PET myocardial perfusion imaging agent. *Journal of Nuclear Cardiology*, *14*, 789–798.

Ziadi, M.C., Dekemp, R.A., Williams, K.A., Guo, A., Chow, B.J., Renaud, J.M. et al. (2011) Impaired myocardial flow reserve on rubidium-82 positron emission tomography imaging predicts adverse outcomes in patients assessed for myocardial ischemia. *Journal of the American College of Cardiology*, *58*, 740–748.

Ziadi, M.C., Dekemp, R.A., Williams, K., Guo, A., Renaud, J.M., Chow, B.J. et al. (2012) Does quantification of myocardial flow reserve using rubidium-82 positron emission tomography facilitate detection of multivessel coronary artery disease? *Journal of Nuclear Cardiology*, *19*, 670–680.